QM/MM study of dislocation—hydrogen/helium interactions in α-Fe

2011 Modelling Simul. Mater. Sci. Eng. 19 065004

(http://iopscience.iop.org/0965-0393/19/6/065004)

Modelling Simul. Mater. Sci. Eng. **19** (2011) 065004 (13pp) doi:10.1088/0965-0393/19/6/065004

QM/MM study of dislocation—hydrogen/helium interactions in α-Fe

Yi Zhao[1,2] **and Gang Lu**[1]

[1] Department of Physics and Astronomy, California State University Northridge, Northridge, CA 91330-8268, USA
[2] Department of Physics, Tsinghua University, Beijing, 100084, People's Republic of China

Received 21 January 2011, in final form 21 April 2011
Published 15 July 2011
Online at stacks.iop.org/MSMSE/19/065004

Abstract

Impurities such as hydrogen (H) and helium (He) interact strongly with dislocations in metals. Using a multiscale quantum-mechanics/molecular-mechanics (QM/MM) approach, we have examined the interactions between the impurities (H and He) with dislocations (edge and screw) in α-Fe. The impurity trapping at the dislocation core is examined by calculating the impurity-dislocation binding energy and the impurity solution energy. We find that in general both H and He prefer the tetrahedral sites at the dislocation core, as well as in the bulk; the exceptions are due to deformed structures at the dislocation cores. Both H and He have a greater solution energy and binding energy to the edge dislocation than to the screw dislocation. The impurity pipe diffusion along the dislocation core is investigated using the QM/MM nudged-elastic-band method. We find that the diffusion barrier along the screw dislocation is lower than the bulk value for both H and He impurities. For the edge dislocation, although H has similar diffusion barriers as in the bulk, He has much higher diffusion energy barriers compared with the bulk. Finally we have examined the impurity effect on the dislocation mobility. We find that both H and He can lower the Peierls energy barrier for the screw dislocation significantly. The H enhanced dislocation mobility is consistent with experimental observations.

(Some figures in this article are in colour only in the electronic version)

1. Introduction

Steels, particularly high strength and ferritic steels, have been used as primary structural materials in vehicles, bridges, naval vessels and fusion reactors, to name but a few. More often than not, these materials are subject to a harsh environment and their mechanical behaviors can be severely influenced by the environment. An extreme example is the ferritic steels used in the first wall of fusion reactors where irradiations could cause displacement damages and induce transmutation products, such as H and He in the steel [1]; these irradiation products are

detrimental to the mechanical properties of the steels. For example, H has long been found as the culprit of the embrittlement of steels at ambient and in particular in corrosive environments [2, 3]; He is known to be responsible for void swelling and mechanical degradation at high temperatures [4–9]. Understanding the interactions between these impurities and intrinsic or irradiation induced structural defects is a key step to develop a comprehensive multiscale model of the impurity effects on the steels. Since α-Fe is the base material and often taken as a first-order model for the advanced steels, in this paper we will examine H and He interactions with dislocations in α-Fe. Because diffusion of H and He impurities in Fe is important for its mechanical properties [9–12], we will study the site preference and the diffusion of these impurities in the dislocations. Furthermore, we will determine the impurity effect on the dislocation mobility by calculating the Peierls energy barrier in the absence/presence of the impurities.

Unfortunately, an accurate determination of impurities diffusion energy barriers along dislocations has remained rather challenging to this date. On the experimental side, the difficulty arises in tracking atomic motion via direct measurements of diffusivity; no such experiment has been reported so far for H and He diffusion in α-Fe dislocations. On the theoretical side, atomistic simulations have only been performed using empirical potentials for Fe. However, the accuracy of these potentials has long been the source of concern and debate; this is hardly surprising considering the enormous challenges to develop *classical* potentials that can capture *quantum magnetism* in addition to describing a myriad of other properties in multicomponent alloys. Nonetheless significant progress has been made to this end [13–17]. On the other hand, although quantum-mechanical simulations are more accurate and reliable than the empirical potentials, they are often computationally too expensive to treat extended defects such as dislocations. To the best of our knowledge, there is no report on the quantum-mechanical study of impurity diffusion in dislocations of Fe. In this paper, we will examine impurity-dislocation interactions in Fe using a quantum-mechanics/molecular-mechanics (QM/MM) approach which describes the dislocation core and the impurities with QM simulations and the long-range dislocation strain field with MM simulations.

2. Methodology and computational models

In the QM/MM approach the system is partitioned into two regions: region I which contains the dislocation core and the impurities is treated with the density function theory (DFT); region II is treated with the empirical EAM potential developed by Shastry *et al* [18]. The EAM potential has been scaled to reproduce the same lattice constant and bulk modules as the corresponding DFT values. The two regions are coupled mechanically and the interaction energy is determined by EAM. Therefore, the total energy of the system can be written as

$$E_{\text{tot}} = E_{\text{I,II}}^{\text{EAM}} + E_{\text{I}}^{\text{DFT}} - E_{\text{I}}^{\text{EAM}}, \tag{1}$$

where the three terms on the right-hand side represent the energy of the entire system calculated by EAM, the energy of region I calculated by DFT and the energy of region I calculated by EAM, respectively. The technical details of the QM/MM method can be found elsewhere [19]. Here we use the Vienna Ab-Initio Simulation Package (VASP) [20] for the DFT calculations; the projected augmentation wave [21] and the generalized gradient approximation (GGA) [22] are used for the pseudopotential and the exchange-correlation potential, respectively. The 1s state for H/He and 3d4s states for Fe are treated as valence states in the calculations. The DFT–GGA method has been successfully applied to describe the interaction of He with a variety of metallic systems [23, 24] including Fe [25–28]. The atomic relaxation is carried out using the conjugate-gradient algorithm with the force convergence criterion of 0.02 eV Å^{-1}.

The diffusion energy barrier and the Peierls energy barrier are calculated using the nudged-elastic-band (NEB) method with the quick-min algorithm [29]. Five and seven intermediate images are used for the diffusion and Peierls barrier calculations, respectively. The same force convergence criterion of 0.02 eV Å^{-1} is also used in the NEB relaxation. Two types of dislocations in Fe are studied in this work, including $\boldsymbol{b} = \frac{1}{2}\langle 1\,1\,1\rangle$ for a screw dislocation and the same Burgers vector for an edge dislocation in the $\{1\,\bar{1}\,0\}$ slip plane. The dimensions of entire simulation box are 280 Å × 280 Å × 7.35 Å in the $[\bar{1}\,1\,0]$ (x), $[\bar{1}\,\bar{1}\,2]$ (y) and $[1\,1\,1]$ (z) directions for the screw dislocation and 280 Å × 280 Å × 6.93 Å in the $[\bar{1}\,1\,0]$ (x), $[1\,1\,1]$ (y) and $[\bar{1}\,\bar{1}\,2]$ (z) directions for the edge dislocation, respectively. Fixed boundary conditions are applied along the x and y directions with the boundary displacement field determined by the isotropic elastic solution of the dislocations. The dislocation line is along the z axis in which the periodical boundary conditions are applied. Note that for the screw dislocation, the z-dimension of the simulation box is three times the minimal periodicity in this direction. Accordingly, the impurities are separated by $\frac{3a}{2}\langle 1\,1\,1\rangle = 7.35$ Å for the screw dislocation and $a\langle 1\,1\,2\rangle = 6.93$ Å for the edge dislocation, which are enough to eliminate chemical interactions between the impurities. The DFT region (region I) for the screw dislocation is a cylinder with a diameter of 16 Å and the cylindrical axis is parallel to the dislocation line. The DFT region for the edge dislocation is a rectangular box of 16 Å × 12 Å along x and y directions, respectively, and the dislocation core is placed at the center. We have also included four additional atomic layers in the DFT region in a test calculation, but observed the identical dislocation core structure—an indication that the DFT region is large enough. The errors at the DFT surfaces are accounted for using a force correction scheme discussed in [19]. The entire system consists of approximately 50 000 atoms with 126 and 111 Fe atoms in the DFT region for the screw and the edge dislocation, respectively; the rest are EAM atoms. Since the vast majority of the atoms are in the EAM region, using EAM to calculate the interaction energy between regions I and II is a reasonable approximation. As a reference, we have also carried out Fe bulk calculations with the same simulation box dimensions as the dislocations. For all QM/MM calculations, a 1 × 1 × 5 Monkhorst–Pack k-point mesh is used. To determine the stacking fault energy, we perform stand-alone DFT calculations [30–32] with a supercell of 54 Fe atoms and the dimensions of 7.3 Å × 12 Å × 7 Å in the $\langle 1\,1\,1\rangle$, $\langle 1\,1\,0\rangle$ and $\langle 1\,1\,2\rangle$ directions, respectively; the shear is along the $\langle 1\,1\,1\rangle$ direction across the $\{1\,1\,0\}$ plane; the Fe atoms are relaxed in the $\langle 1\,1\,0\rangle$ direction and the impurity atom is fully relaxed. The k-point mesh for the stacking fault energy calculations is 5 × 3 × 5. In all DFT-VASP calculations, we have used the Methfessel–Paxton smearing scheme with the smearing width of 0.5 eV. The energy cutoff of all VASP calculations is 300 eV. A larger energy cutoff of 400 eV has also been tested in several cases which yield energy barrier differences less than 3 meV for He and H diffusion in Fe, compared with the smaller energy cutoff of 300 eV.

3. Results and discussion

3.1. Dislocation core structure and magnetization

In this section, we focus on pure Fe in an attempt to correlate the dislocation strain field to the local magnetic moments on the Fe atoms, relative to the corresponding bulk values. The QM/MM simulations predict a compact and non-degenerate core structure for the screw dislocation which agrees well with other simulation results [33, 34]. The local magnetic moment is calculated using VASP and the Wigner–Seitz radius for Fe is 1.3 Å. The averaged local strain field plotted in figures 1(c) and (d) is calculated as $\epsilon_i = \frac{1}{N_{nn}}\sum_j \frac{r_{ij}-r_{ij}^0}{r_{ij}^0}$, where i, j is

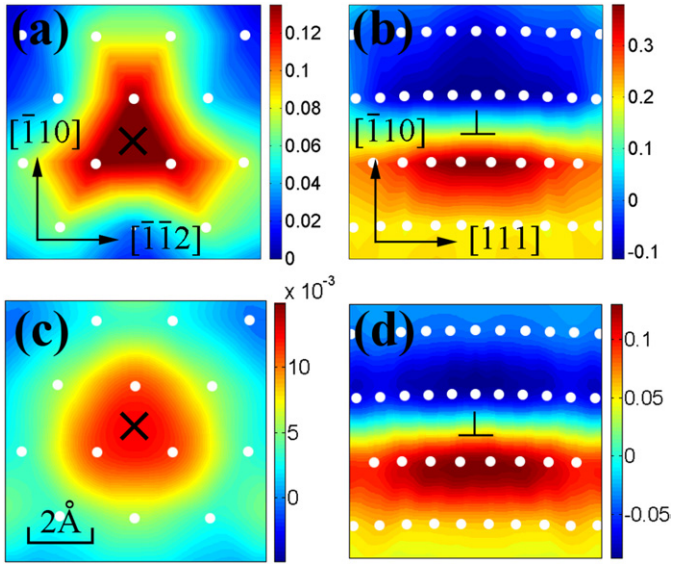

Figure 1. Magnetic moment (upper panel) and local strain field (lower panel) of the screw (left) and edge (right) dislocations. The magnetic moment on the core atoms is plotted with respect to the corresponding bulk value and the unit is μ_b. The Fe atoms projected onto the (1 1 1) plane for the screw dislocation and onto the (1 1 2) plane for the edge dislocation are shown in white dots. A cross (an inverted 'T') symbol is used to represent the screw (edge) dislocation.

the atom index and j sums over the nearest neighbors of the atom i; N_{nn} is the number of the nearest neighbors. r_{ij} and r_{ij}^0 are the interatomic distances in the dislocation and the perfect lattice, respectively. For screw dislocation we find an increase in the magnetic moment (the maximum increase is 0.14 μ_b) at the dislocation core comparing with the bulk value. For the edge dislocation, there is an increase in the magnetic moment (the maximum increase is 0.40 μ_b) at the tension side of the slip plane and a decrease in the magnetic moment (the maximum decrease is 0.13 μ_b) at the compression side of the slip plane. The correlation between the dislocation strain field and the magnetic moments is clearly evident in figure 1. We have also calculated the bulk magnetic moment as a function of strain in figure 2 and found a monotonic increase in the magnetic moment as a function of strain (from compression to tensile). The magnetization-volume correlation observed in bulk Fe agrees well with the earlier work by others [35]. The correlation observed in bulk Fe is consistent with the results in the dislocations. The relaxed dislocation structures are then used as the starting configurations in which the impurities will be introduced.

3.2. Site preference

In order to evaluate the site preference of the impurities in bulk and the dislocation core, we calculate the impurity solution energy with the QM/MM method as follows:

$$E^{\mathrm{s}}_{\mathrm{X,Y}} = E_{\mathrm{X+Y}} - E_{\mathrm{X}} - E_{\mathrm{Y}}. \tag{2}$$

Here X could stand for bulk, edge, screw dislocation respectively and Y represents either He or H impurity. The three energy contributions are the energy of X in the presence of the impurity Y, the energy of X in the absence of any impurity, and the energy of the impurity Y by itself. The more negative the solution energy, the stronger the binding between X and Y

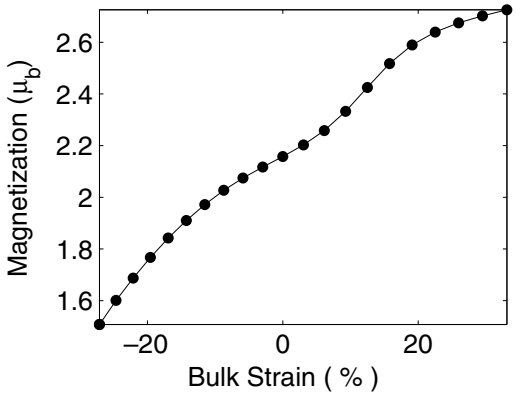

Figure 2. The bulk magnetic moment as a function of the applied strain.

(or the site is more preferred by the impurity). In bulk Fe, we find that both H and He prefer the tetrahedral (T-) site over the octahedral (O-) site, consistent with other *ab initio* and atomistic results [26, 36–38]. In dislocations, however, the situations are more complicated owing to the lattice distortions at the core. For the screw dislocation, although T-sites are still preferred in general, some O-sites become more favourable for He as shown in figure 3(*b*); these O-sites are more stable than their adjacent T-sites because of the larger space available along the vertical direction (cf figure 3(*a*)). Another exception is 'pyramidal' (P-) sites in which H prefers to occupy; these P-sites are closer to the O-sites than to the T-sites. For the edge dislocation, H prefers to occupy the T-sites and He favours the O-sites at the tension side of the slip plane. The configurations corresponding to the lowest solution energies are as follows: (1) He atom occupies a T-site in the screw dislocation core; (2) H atom occupies a P-site in the second shell of the screw dislocation core; (3) He at the O-site in the first Fe layer on the tension side of the edge dislocation; (4) H atom at the T-site between the first and the second Fe layers on the tension side of the edge dislocation (the energy is only 0.02 eV lower than in the slip plane). The energies of the most stable sites are summarized in table 1. The solution energy of H is negative in both bulk and the dislocations, while it is positive for He in both bulk and the dislocations. Particularly, $E^{\mathrm{s}}_{\mathrm{bulk,He}}$ is 4.21 eV, consistent with the *ab initio* result of 4.37 eV reported by others [25, 26, 39]. The large positive value of $E^{\mathrm{s}}_{\mathrm{X,He}}$ and the negative value of $E^{\mathrm{s}}_{\mathrm{X,H}}$ suggest that He is not bonded to the Fe matrix, while H is strongly bonded to Fe atoms. As shown in figure 4, strong ionic bonding is clearly visible between H and Fe atoms, while there is very little bonding between He and Fe atoms.

We have also calculated the impurity binding (or segregation) energy to the dislocation core which is defined as the solution energy difference between the bulk and the dislocations: $E^{\mathrm{b}}_{\mathrm{dis,Y}} = E^{\mathrm{s}}_{\mathrm{dis,Y}} - E^{\mathrm{s}}_{\mathrm{bulk,Y}}$. Here 'dis' could be either edge or screw and Y represents H or He. The lower the binding/segregation energy, the more stable the impurity at the dislocation core; the negative value of the binding/segregation energy indicates that the impurity prefers to segregate to the dislocation core as opposed to staying in the bulk. The lowest binding energy of H to the screw and the edge dislocation is −0.27 eV and −0.47 eV respectively; the corresponding value for He is −0.49 eV and −1.66 eV, respectively. Therefore, both H and He are energetically most stable in the edge dislocation, less stable in the screw dislocation and least stable in the bulk. This energetic trend may be understood from the volume consideration: both H and He impurities expand the volume of the occupied tetrahedron, by 14% and 35%, respectively. Since the edge dislocation has more open space than the screw dislocation and

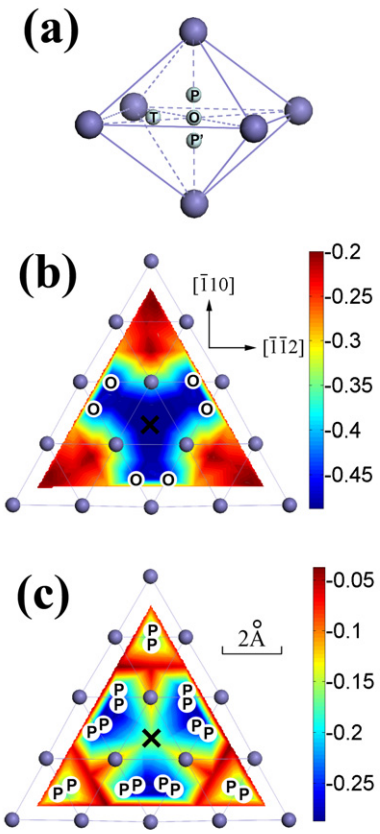

Figure 3. (*a*) The schematic diagram of the possible interstitial sites. (*b*) The binding energy diagram of He at the screw dislocation core. (*c*) The binding energy of H at the screw dislocation core. Blue spheres represent Fe atoms and 'T', 'O' and 'P' stand for tetrahedral, octahedral and pyramidal sites, respectively. In (*b*) and (*c*), only the exceptional cases are shown. The energy unit is eV.

the bulk, the binding energy is lower. It is worth noting that the binding energy of He to the screw and edge dislocation is −1.05 eV and −2.29 eV, respectively, obtained with an empirical potential [40].

3.3. Impurity diffusion along the screw dislocation

First, we calculate the impurity diffusion energy barrier in the bulk with the QM/MM method. We find that the diffusion energy barrier is 0.09 and 0.05 eV for H and He, respectively, between two adjacent bulk tetrahedral sites; these numbers agree very well with the corresponding values (0.1 eV for H and 0.06 eV for He) obtained by others using *ab initio* calculations [17, 25, 41]. Next, we examine the impurities pipe diffusion along the screw dislocation with the QM/MM method. Both H and He diffuse between adjacent tetrahedral sites along the dislocation line, as shown in figure 5(*b*). We have focused on two different diffusion 'pipes': (A) along the dislocation core in which all tetrahedra are equally distorted and (B) the 'pipe' next to the core in which the distortions are the not the same. The two pipes are displayed in figure 5(*a*) using the standard differential displacement map [42]. The diffusion barriers are summarized

Table 1. Solution energy, binding energy and diffusion energy barriers (E^{d}) for H and He in bulk Fe, screw dislocation and edge dislocation. The energy unit is eV. Superscripts A and B refer to pipe A and B in figure 5(*a*). Superscript $\parallel$ or $\perp$ indicates that the diffusion path is parallel or perpendicular to the $[\bar{1}\,\bar{1}\,5]$ direction, as shown in figure 6.

Energy		H		He	
E^{s}	bulk	−2.33		4.21	
	screw	−2.60		3.72	
	edge	−2.80		2.55	
E^{b}	screw	−0.27		−0.49	
	edge	−0.47		−1.66	
E^{d}	bulk	0.09		0.05	
	screw	0.035^{A}	0.63^{B}	0.038^{A}	0.073^{B}
	edge	$0.09^{\parallel}$	$0.15^{\perp}$	$0.15^{\parallel}$	$0.48^{\perp}$

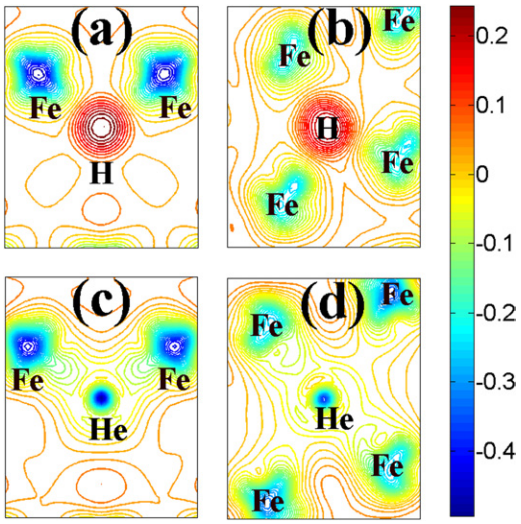

Figure 4. Bonding charge density of the interstitial H and He atoms with the adjacent Fe atoms. (*a*) H at the tetrahedral site of the screw dislocation. (*b*) H at the tetrahedral site of the edge dislocation. (*c*) He at the octahedral site of the screw dislocation. (*d*) He at the octahedral site of the edge dislocation. The unit is electron $Å^{-3}$.

in table 1. We find that both H and He have a lower diffusion energy barrier along pipe A, which is 0.035 eV and 0.038 eV, respectively. These barriers are smaller than the bulk values because there is more space along the dislocation core for the impurities. The diffusion barrier of He is much smaller than the result (0.4 eV) obtained using an empirical potential [43]. The diffusion barrier along the 'pipe' B is 0.63 eV and 0.073 eV for H and He, respectively. Note that H diffuses through both T-sites and P-sites while He diffuses via both the T-sites and O-sites along the pipe B. We have also carried out a molecular-dynamics (MD) simulation for the screw dislocation with He impurity using the QM/MM approach. The temperature of the system is 800 K and controlled by the Berendson thermostat [44]. The simulated time is 1 ps consisting of 1000 MD steps; during the simulation, the He atom has diffused away from the its original position by approximately 6 Å, but still remains in the core region. The MD results suggest that the diffusion energy barriers in the core are in the order of the simulated temperature (0.07 eV) for the screw dislocation.

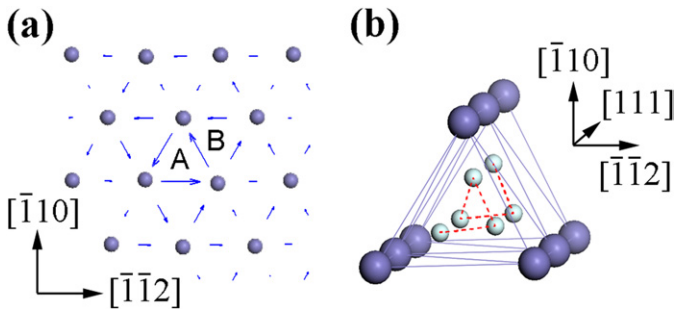

Figure 5. Atomic structure and impurity diffusion paths along the screw dislocation. (*a*) The differential displacement map of the screw dislocation. (*b*) The diffusion path represented by the red dashed curve passing through the tetrahedral sites along 'pipe A' for both H and He. Fe atoms and the tetrahedral sites are shown in large and small spheres, respectively.

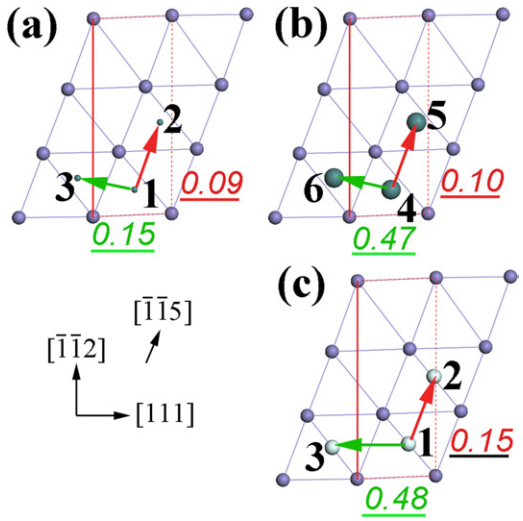

Figure 6. Elementary diffusion hops along the edge dislocation: (*a*) H diffusion between the first and the second atomic layer at the tension side of the slip plane. (*b*) H diffusion in the slip plane. (*c*) He diffusion in the first atomic layer at the tension side of the slip plane. Only the first Fe layer on the tension side of the slip plane is shown in spheres. A unit cell of the slip plane is shown as a red rectangular box. The dislocation line is indicated as a red solid line. Atoms closer to the slip plane are shown in larger spheres. The diffusion energy barriers are labeled beside the corresponding diffusion paths and the energy unit is eV.

3.4. Impurity diffusion along the edge dislocation

The diffusion along the edge dislocation is more complicated because the edge dislocation line is along the [$\bar{1}$ $\bar{1}$ 2] direction whose periodicity is 6.93 Å, much larger than that of the screw dislocation (2.45 Å). Since the most stable sites of the impurities are located along the [$\bar{1}$ $\bar{1}$ 5] direction which is tilted at 22° with respect to the dislocation line, we project the diffusion path onto two perpendicular directions: (1) diffusion along the [$\bar{1}$ $\bar{1}$ 5] direction; (2) diffusion perpendicular to the [$\bar{1}$ $\bar{1}$ 5] direction; they are shown in red and green arrows, respectively, in figure 6. In figure 6(*a*), '1' and '2' are two equivalent tetrahedral sites along the [$\bar{1}$ $\bar{1}$ 5] direction and '1' and '3' are two equivalent tetrahedral sites perpendicular to [$\bar{1}$ $\bar{1}$ 5]. A diffusion path

along the dislocation line can be regarded as a combination of the two elementary hops—'1–2' and '1–3' hops.

For H diffusion, we consider two types of occupancies which have about the same solution energy: (i) interstitials between the first and second layer at the tension side of the slip plane, see figure 6(*a*) and (ii) interstitials at the slip plane, see figure 6(*b*). The H diffusion barrier along $[\bar{1}\ \bar{1}\ 5]$ in case (i) and (ii) is 0.09 eV and 0.10 eV, respectively, which is the very close to the bulk values. The H diffusion barrier perpendicular to the $[\bar{1}\ \bar{1}\ 5]$ direction is 0.15 eV in case (i) and a very high barrier of 0.47 eV in case (ii). The difference is mainly due to the atomic structures of (i) and (ii), which are very different for the edge dislocation. For He diffusion, the diffusion barriers are shown in figure 6(*c*) of 0.15 eV and 0.48 eV, respectively, for the two elementary hops. The He diffusion energy barriers along the edge dislocation are much higher than those in the bulk and the screw dislocation for two reasons: (1) in the edge dislocation, He prefers the O-sites which are at the same plane of Fe atoms along the diffusion path. Therefore, He has to 'squeeze' between the neighboring Fe atoms, resulting higher diffusion barriers. On the other hand, in both bulk and the screw dislocation, He prefers the T-sites, which are not at the same plane of Fe atoms along the diffusion path, thus the energy barriers are lower. (2) He is energetically more stable at the edge dislocation core than in the bulk or the screw dislocation as shown in table 1. Hence comparing in the bulk and the screw dislocation, He has a greater tendency to stay put at the larger O-sites in the edge dislocation as opposed to diffusing out.

3.5. Impurity effect on dislocation mobility

Finally, we address the mobility of the screw dislocation by calculating its Peierls energy barrier, which is the minimum energy that a straight dislocation has to overcome in order to move in a crystal. We focus on the screw dislocation here because its mobility is much lower than that of the edge dislocation, hence its mobility is more relevant to the overall mobility of a curved dislocation or a dislocation loop. We use the QM/MM NEB method to estimate the Peierls barrier. The dislocation is placed at two adjacent 'easy' positions as the initial and final state, as shown in figures 7(*a*) and (*c*) respectively. The minimal energy path is found to be in the {1 1 0} plane, which is consistent with experiments [45]. The saddle point configuration (figure 7(*b*)) has a 'none-split' core structure, which is in agreement with other DFT calculations, but different from the 'split-core' structure observed using empirical potentials [46, 47]. The none-split core is very close to the 'hard' core configuration while the split-core means that the dislocation spreads into two 'easy' core configurations. The minimal energy path profile has a single-peak, consistent with the DFT-SIESTA calculations by Ventelon *et al* [46]. The Peierls energy barrier for the pure screw dislocation is 0.06 eV/b, higher than the results (0.027 eV/b and 0.033 eV/b) of Ventelon *et al*. The difference might be attributed to following reasons: first, we use the QM/MM method while Ventelon *et al* used both cluster and dipole models. In the cluster model, the dislocation is inevitably influenced by the surfaces; in the dipole model, although the net Burgers vector is zero, the dislocations nonetheless still interact with each other if the computational cell is not large enough—a typical situation for DFT calculation. In addition, any symmetry breaking event at the dislocation core (such as asymmetric core splitting and impurity position) and/or nonlinearity could lead to errors in the periodic simulations. However, it is not clear to what extend Ventelon *et al* calculation might suffer from the fictitious interactions. In the QM/MM method, these two problems do not arise. Second, our VASP calculation yields a unstable stacking fault energy γ_{us} of 1.03 J m^{-2} or 64 meV Å^{-2} along the $\langle 1\ 1\ 1\rangle$ direction in the {1 1 0} plane, which agrees well with other DFT results using plane-wave basis [48, 49]. However, our numbers are

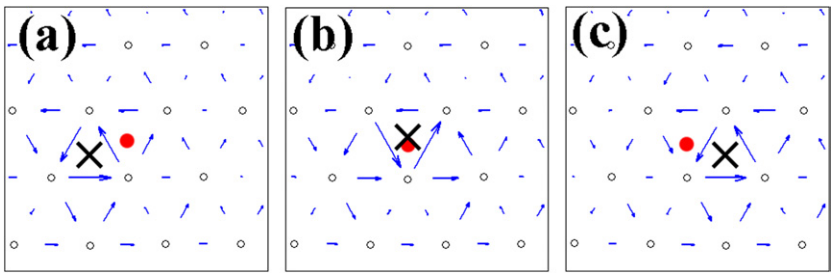

Figure 7. The differential displacement maps of the screw dislocation moving along the minimum energy path: (*a*) initial structure, (*b*) saddle point and (*c*) final structure. The dislocation core is represented by the cross and the position of the impurity is indicated by a red dot. The orientations are the same as figure 5(*a*).

higher than those reported by Ventelon *et al* using the DFT-SIESTA method (0.77 J m^{-2} or 48 meV Å^{-2}). Therefore, the different DFT methods (VASP versus SIESTA) themselves could also contribute to the different Peierls barriers. Although we suspect that the different basis sets—plane-waves versus localized atomic basis—are the source of the discrepancies, more studies are needed to nail this down. Last, different convergency criteria used in the NEB calculations could also attribute to the discrepancies. In the Peierls energy calculations with impurities, one impurity atom (H or He) is introduced at the dislocation core. In the presence of the impurities, the Peierls barrier becomes 0.03 eV/b for H and 0.02 eV/b for He impurity, respectively, shown in figure 8(*a*). The reduction in the Peierls energy barriers is significant and can be explained from the calculated γ energy shown in figure 8(*b*). With 1 impurity atom per $\langle 1\,1\,2\rangle \times \frac{3}{2}\langle 1\,1\,1\rangle$ cell (49 Å^2 in area), H and He lower γ_{us} by 0.08 J m^{-2} (or 5 meV Å^{-2}) and 0.16 J m^{-2} (or 10 meV Å^{-2}), respectively. In the presence of H, the covalent Fe–Fe bonding across the slip plane is significantly disrupted and Fe–H ionic bonding is formed at its expense. Since the ionic Fe–H bonding across the slip plane resembles the formation of positively and negatively charged plates, the energy cost is not as sensitive to the shear as for the covalent Fe–Fe bonding. Hence the γ-energy in the presence of H is lower. This effect is similar to what has been observed in Al [32]. On the other hand, the presence of He swells the surrounding Fe lattice—the interlayer distance across the slip plane increases by 0.3 Å. Since there is very little bonding between He and Fe, the cohesion across the slip plane is significantly weakened and thus is insensitive to the relative shear across the slip plane. The reduced Peierls energy barrier in the presence of H is also consistent with H enhanced local plasticity phenomenon which has been observed in many metals, including Fe [2].

4. Conclusion

Using the multiscale QM/MM approach, we have examined the interactions between H and He impurities with the dislocations in α-Fe. The impurity trapping at the dislocation core is investigated by calculating the impurity-dislocation solution energy and the impurity binding energy to the dislocation cores. We find that in general both H and He prefer the tetrahedral sites at the dislocation core, as well as in the bulk; the exceptions are due to the deformed structures at the dislocation cores. Both H and He have a greater solution energy and binding energy to the edge dislocation than to the screw dislocation. The impurity pipe diffusion along the dislocation core is examined using the QM/MM NEB method. We find that the diffusion energy barrier along the screw dislocation is lower than the bulk value for both H

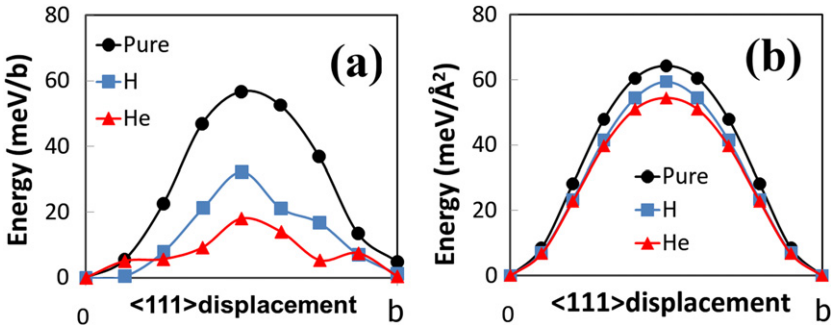

Figure 8. (*a*) The Peierls energy barrier of the screw dislocation. (*b*) The γ-energy of pure Fe and Fe with H or He impurities.

and He impurities. For the edge dislocation, although H has similar diffusion barriers than the bulk, He has much higher diffusion energy barriers compared with the bulk. Finally we have examined the impurity effect on the dislocation mobility. We find that both H and He can lower the Peierls energy barrier for the screw dislocation significantly. The H enhanced dislocation mobility is consistent with the experimental observations.

Acknowledgments

The work was supported by the Office of Naval Research and the Department of Energy. The computational facility was supported by NSF-MRI. We thank Professor Nasr Ghoniem for inspiring discussions and encouragement.

References

[1] Schäublin R and Baluc N 2007 Radiation damage in ferritic/martensitic steels for fusion reactors: a simulation point of view *Nucl. Fusion* **47** 1690
[2] Myers S M *et al* 1992 Hydrogen interactions with defects in crystalline solids *Rev. Mod. Phys.* **64** 559–617
[3] Nagumo M 2001 Advances in physical metallurgy and processing of steels. function of hydrogen in embrittlement of high-strength steels *ISIJ Int.* **41** 590–8
[4] Ishizaki T, Xu Q, Yoshiie T, Nagata S and Troev T 2002 The effect of hydrogen and helium on microvoid formation in iron and nickel *J. Nucl. Mater.* **307–311** 961–5
[5] Samaras M 2009 Multiscale modelling: the role of helium in iron *Mater. Today* **12** 46–53
[6] Hunn J D, Lee E H, Byun T S and Mansur L K 2000 Helium and hydrogen induced hardening in 316LN stainless steel *J. Nucl. Mater.* **282** 131–6
[7] Hashimoto N, Hunn J D, Byun T S and Mansur L K 2003 Microstructural analysis of ion-irradiation-induced hardening in inconel 718 *J. Nucl. Mater.* **318** 300–6
[8] Gelles D S 2000 On quantification of helium embrittlement in ferritic/martensitic steels *J. Nucl. Mater.* **283–287** 838–40
[9] Ryazanov A, Braski D, Schroeder H, Trinkaus H and Ullmaier H 1996 Modeling the effect of creep on the growth of helium bubbles in metals during annealing *J. Nucl. Mater.* **233–237** 1076–9
[10] Domain C 2006 *Ab initio* modelling of defect properties with substitutional and interstitials elements in steels and Zr alloys *J. Nucl. Mater.* **351** 1–19
[11] Fu C C, Willaime F and Ordejón P 2004 Stability and mobility of mono- and di-interstitials in α-Fe *Phys. Rev. Lett.* **92** 175503
[12] Zhang Y, Feng W Q, Liu Y L, Lu G H and Wang T M 2009 First-principles study of helium effect in a ferromagnetic iron grain boundary: energetics, site preference and segregation *Nucl. Instrum. Methods Phys. Res.* B **267** 3200–3

[13] Mendelev M I, Han S, Srolovitz D J, Ackland G J, Sun D Y and Asta M 2003 Development of new interatomic potentials appropriate for crystalline and liquid iron *Phil. Mag.* **83** 3977
[14] Ramasubramaniam A, Itakura M and Carter E A 2009 Interatomic potentials for hydrogen in α–iron based on density functional theory *Phys. Rev.* B **79** 174101
[15] Malerba L *et al* 2010 *Ab initio* calculations and interatomic potentials for iron and iron alloys: achievements within the perfect project *J. Nucl. Mater.* **406** 7–18
[16] Gao N, Samaras M and Van Swygenhoven H 2010 A new Fe–He pair potential *J. Nucl. Mater.* **400** 240–4
[17] Stewart D M, Osetsky Y N, Stoller R E, Golubov S I, Seletskaia T and Kamenski P J 2010 Atomistic studies of helium defect properties in bcc iron: comparison of He–Fe potentials *Phil. Mag.* **90** 935–44
[18] Shastry V and Farkas D 1996 Molecular statics simulation of fracture in α-iron *Modell. Simul. Mater. Sci. Eng.* **4** 473
[19] Zhao Y, Wang C, Peng Q and Lu G 2010 Error analysis and applications of a general QM/MM approach *Comput. Mater. Sci.* **50** 714–19
[20] Kresse G and Hafner J 1994 *Ab initio* molecular-dynamics simulation of the liquid-metal–amorphous-semiconductor transition in germanium *Phys. Rev.* B **49** 14251–69
[21] Blöchl P E 1994 Projector augmented-wave method *Phys. Rev.* B **50** 17953–79
[22] Perdew J P, Burke K and Ernzerhof M 1996 Generalized gradient approximation made simple *Phys. Rev. Lett.* **77** 3865–8
[23] Petersen M, Wilke S, Ruggerone P, Kohler B and Scheffler M 1996 Scattering of rare-gas atoms at a metal surface: evidence of anticorrugation of the helium-atom potential energy surface and the surface electron density *Phys. Rev. Lett.* **76** 995–8
[24] Jean N, Trioni M I, Brivio G P and Bortolani V 2004 Corrugating and anticorrugating static interactions in helium-atom scattering from metal surfaces *Phys. Rev. Lett.* **92** 013201
[25] Fu C C and Willaime F 2005 *Ab initio* study of helium in α-Fe: dissolution, migration, and clustering with vacancies *Phys. Rev.* B **72** 064117
[26] Seletskaia T, Osetsky Y, Stoller R E and Stocks G M 2005 Magnetic interactions influence the properties of helium defects in iron *Phys. Rev. Lett.* **94** 046403
[27] Ventelon L, Wirth B and Domain C 2006 Helium-self-interstitial atom interaction in α-iron *J. Nucl. Mater.* **351** 119–32
[28] Zu X T, Yang L, Gao F, Peng S M, Heinisch H L, Long X G and Kurtz R J 2009 Properties of helium defects in bcc and fcc metals investigated with density functional theory *Phys. Rev.* B **80** 054104
[29] Henkelman G, Uberuaga B P and Jónsson H 2000 A climbing image nudged elastic band method for finding saddle points and minimum energy paths *J. Chem. Phys.* **113** 9901–4
[30] Vitek V 1974 Theory of the core structures of dislocations in body-centred-cubic metals *Cryst. Latt. Def.* **5** 1–34
[31] Lu G, Kioussis N, Bulatov V V and Kaxiras E 2000 Generalized-stacking-fault energy surface and dislocation properties of aluminum *Phys. Rev.* B **62** 3099–108
[32] Lu G, Orlikowski D, Park I, Politano O and Kaxiras E 2002 Energetics of hydrogen impurities in aluminum and their effect on mechanical properties *Phys. Rev.* B **65** 064102
[33] Domain C and Monnet G 2005 Simulation of screw dislocation motion in iron by molecular dynamics simulations *Phys. Rev. Lett.* **95** 215506
[34] Clouet E, Ventelon L and Willaime F 2009 Dislocation core energies and core fields from first principles *Phys. Rev. Lett.* **102** 055502
[35] Elsässer C, Zhu J, Louie S G, Fähnle M and Chan C T 1998 *Ab initio* study of iron and iron hydride: I. cohesion, magnetism and electronic structure of cubic Fe and FeH *J. Phys. Condens. Matter* **10** 5081
[36] Sanchez J, Fullea J, Andrade M C and de Andres P L 2010 *Ab initio* molecular dynamics simulation of hydrogen diffusion in α-iron *Phys. Rev.* B **81** 132102
[37] Ramasubramaniam A, Itakura M, Ortiz M and Carter E A 2008 Effect of atomic scale plasticity on hydrogen diffusion in iron: quantum mechanically informed and on-the-fly kinetic Monte Carlo simulations *J. Mater. Res.* **23** 2757–73
[38] Jiang D E and Carter E A 2004 Diffusion of interstitial hydrogen into and through bcc Fe from first principles *Phys. Rev.* B **70** 064102
[39] Seletskaia T, Osetsky Yu N, Stoller R E and Stocks G M 2006 Calculation of helium defect clustering properties in iron using a multi-scale approach *J. Nucl. Mater.* **351** 109–18
[40] Kurtz R J, Heinisch H L and Gao F 2008 Modeling of He-defect interactions in ferritic alloys for fusion *J. Nucl. Mater.* **382** 134–42
[41] Ortiz C J, Caturla M J, Fu C C and Willaime F 2007 He diffusion in irradiated α-Fe: An *ab initio*-based rate theory model *Phys. Rev.* B **75** 100102

[42] V Vitek, Perrin R C and Brown D K 1970 Core structure of $1/2(1\,1\,1)$ screw dislocations in bcc crystals *Phil. Mag.* **21** 1049
[43] Heinisch H L, Gao F and Kurtz R J 2007 Atomistic modeling of helium interacting with screw dislocations in α-Fe *J. Nucl. Mater.* **367–370** 311–15
[44] Berendsen H J C, Postma J P M, van Gunsteren W F, DiNola A and Haak J R 1984 Molecular dynamics with coupling to an external bath *J. Chem. Phys.* **81** 3684–90
[45] Spitzig W A and Keh A S 1970 The effect of orientation and temperature on the plastic flow properties of iron single crystals *Acta. Metall.* **18** 611–22
[46] Lisa Ventelon and Willaime F 2007 Core structure and peierls potential of screw dislocations in α-Fe from first principles: cluster versus dipole approaches *J. Comput. Aided Mater. Des.* **14** 85–94
[47] Gilbert M R and Dudarev S L 2010 *Ab initio* multi-string Frenkel–Kontorova model for a $b = a/2[1\,1\,1]$ screw dislocation in bcc iron *Phil. Mag.* **90** 1035–61
[48] Frederiksen S L and Jacobsen K W 2003 Density functional theory studies of screw dislocation core structures in bcc metals *Phil. Mag.* **83** 365–75
[49] Ventelon L and Willaime F 2010 Generalized stacking-faults and screw-dislocation core-structure in bcc iron: a comparison between *ab initio* calculations and empirical potentials *Phil. Mag.* **90** 1063–74